NASA TM X-137

TECHNICAL MEMORANDUM
X-137

FLIGHT BEHAVIOR OF THE X-2 RESEARCH AIRPLANE TO A MACH NUMBER OF 3.20 AND A GEOMETRIC ALTITUDE OF 126,200 FEET

By Richard E. Day and Donald Reisert

High-Speed Flight Station
Edwards, Calif.

NATIONAL AERONAUTICS AND SPACE ADMINISTRATION

WASHINGTON

September 1959
Declassified March 18, 1960

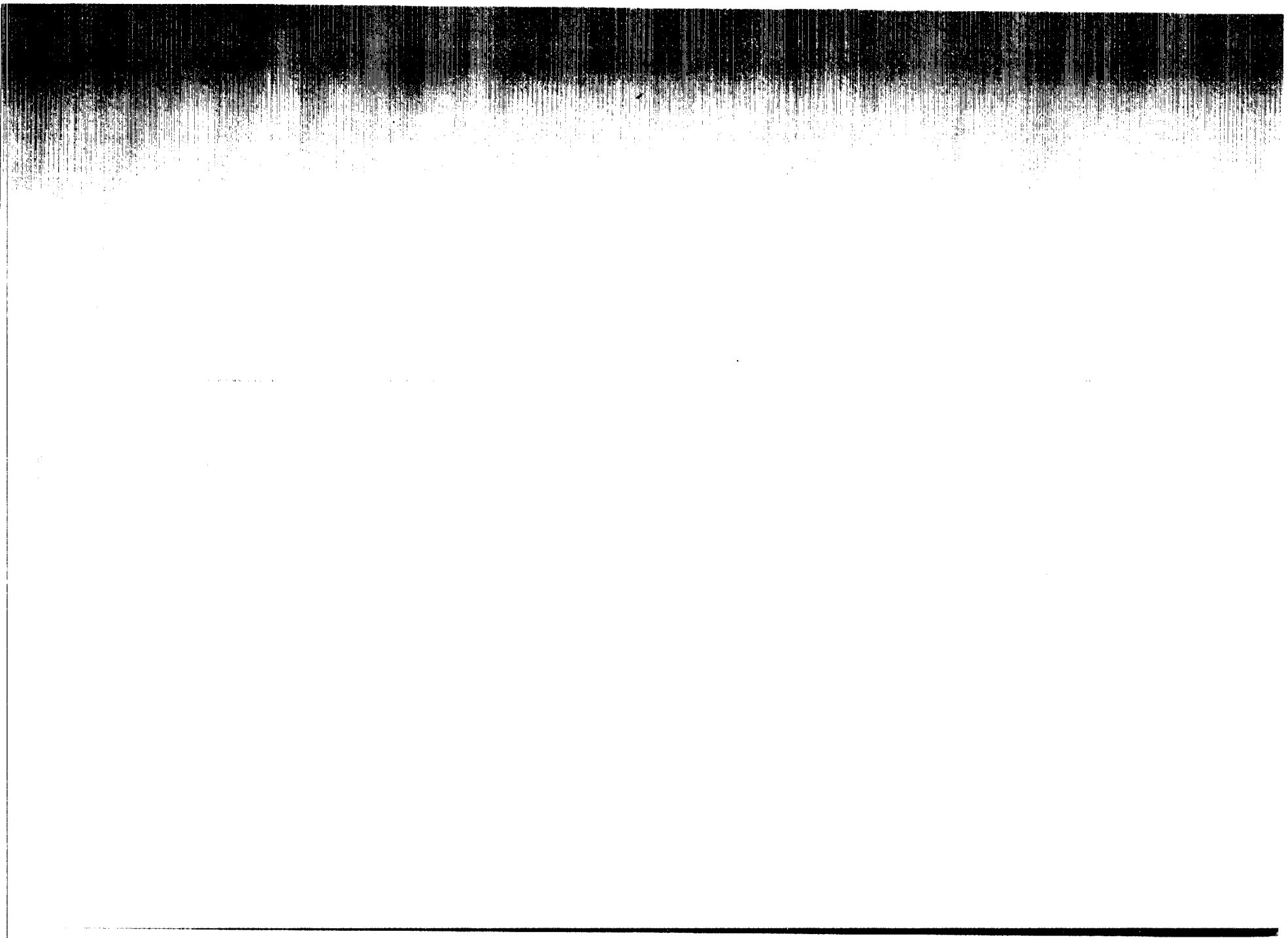

Airspeed
Pressure altitude
Angle of attack and angle of sideslip
Pitching, rolling, and yawing angular velocities
Stabilizer, left-aileron, and rudder deflections
Longitudinal, transverse, and normal accelerations

All instruments were synchronized by a common timer. Geometric altitude was calculated from U. S. Air Force radar data. An NASA high-speed pitot-static tube was mounted on a boom forward of the nose of the airplane. A position-error calibration of the airspeed system was made early in the flight program by using the techniques of reference 5. The calibration extended from a Mach number of 0.65 to a Mach number of 2.30; the error is approximately ±0.02 at subsonic speeds and ±0.01 for supersonic speeds. Pressure-lag measurements were not made on the static- or dynamic-pressure systems because of the loss of the airplane. The pressure-lag error is appreciable in the high-altitude portion of the program, but of less importance during the high Mach number flights. The pressure-altitude data presented herein are based on reference 6. All other quantities were corrected for instrumentation errors.

TEST PROCEDURE

To guide the flight program, a five-degree-of-freedom analog simulation was performed of the airplane stability and control characteristics throughout the estimated performance envelope. The analog computer used for this study was located at the Air Force Flight Test Center, Edwards, Calif. Wind-tunnel and theoretical values of the aerodynamic derivatives (refs. 3, 7, 8, and manufacturer's estimates) were used until flight derivatives were obtained. For simulation at increasingly higher speeds, it was necessary to extrapolate the values of the flight derivatives. During several buildup flights to maximum Mach number, flight maneuvers to obtain aerodynamic derivatives were accomplished up to a Mach number of 2.4. Consequently, all data used in simulating flight at higher Mach numbers were extrapolated from this Mach number. Before each flight, the X-2 pilots were given time at the controls of the simulator. The characteristics of the airplane were demonstrated over the proposed speed increment, and, the more important aerodynamic derivatives were varied over the lift range at the advanced speeds.

RESULTS AND DISCUSSION

Only the presentation and analysis of one high-altitude flight and two high Mach number flights are discussed, inasmuch as the peak performance of the X-2 airplane was attained in these flights.

The drop conditions of an indicated airspeed of 225 mph and an altitude of 30,000 feet were the same for all flight plans. The rocket engine was started approximately 6 seconds after drop, and the airplane was rotated and allowed to accelerate along an average flight-path angle of about 30°. An indicated airspeed not exceeding 350 mph was maintained in order to obtain lift coefficients for minimum drag. All flights progressed along this path to the point of departure for either high-altitude or high-speed trajectories.

High-Altitude Performance

The analog investigation indicated that the airplane would be controllable throughout the expected altitude range.

Figure 4 shows a time history of flight A, the maximum altitude flight made with the X-2 airplane. The launch and acceleration along the minimum-drag climb progressed satisfactorily so that at a Mach number of about 1.25 and an altitude of 56,000 feet (t = 81.5) full airplane nose-up control was applied, increasing the flight-path angle to a maximum of about 38° and normal acceleration to a maximum of 1.2g. Burnout occurred at a pressure altitude of 104,000 feet, at which point the longitudinal acceleration had increased to 1.45g. After burnout, the airplane followed a semiballistic trajectory with the normal acceleration approaching 0g for a sustained period. The normal acceleration dropped to a minimum of 0.084g (t = 174 sec) and was less than 0.2g for approximately 40 seconds. The airplane did not attain 0g about all three axes.

As the trajectory approached the peak, the pilot applied nose-down stabilizer. This control input initiated a large oscillation, with the angle of attack changing a maximum of 6° with a period of 6 seconds. The pilot was not aware of this oscillation inasmuch as the period was long and produced no appreciable change in the normal acceleration, and the flight path was approximately 20° so that the horizon was not visible for reference. The longitudinal control was effective for attitude control, as shown by the change in angle of attack with control application; however, the flight path was not noticeably changed.

The maximum indicated pressure altitude attained was 119,800 feet at a Mach number of 1.7, with a corresponding radar-measured geometric altitude of 126,200 feet. A comparison of these altitudes is shown in the time history of figure 4. At the peak altitude, the airplane experienced a free-stream dynamic pressure of 19.1 pounds per square foot at a static pressure of 9.4 pounds per square foot. A constant angle-of-attack descent was made by holding full aft stick to a normal acceleration of about 3g, after which the stabilizer deflection was gradually decreased, with the peak normal acceleration being 3.5g. The pullout was completed at an altitude of 40,000 feet near a Mach number of 1.

The system-pressure lag discussed in the section entitled "INSTRUMENTATION" is shown in figure 4. At the pressure altitude of 110,000 feet the Mach number during the ascent was 1.7; for this altitude during the descent the indicated Mach number is increased by 0.2.

As shown by the oscillations of the longitudinal quantities in figure 4, the longitudinal period increases from about 1.5 seconds at 40,000 feet to about 6 seconds near 120,000 feet. The lateral period increases to a maximum of approximately 10 seconds at the peak altitude. Although the damping of both the longitudinal and lateral modes was poor, it was always positive and the pilot was not affected by the oscillations because of the long periods and low accelerations.

The angle of sideslip shows evidence of an asymmetric power condition. At burnout (t = 142.8), the angle changed from 5.5° right to 3° left as a result of the removal of an equivalent nose-left yawing moment from the airplane. (The data show that the change to power-off had no effect on the pitching motions of the airplane.) This asymmetric power condition caused a left rolling motion; however, the pilot reported that the rolling motion was terminated by control action at an appreciable left-bank angle and the descent was made in this condition.

High Mach Number Performance

The analog investigation indicated that at the higher Mach numbers (2.7 to 3.2) the most pessimistic derivative extrapolations resulted in stable flight for trim lift ($\alpha \approx 2°$), but deteriorated into a directional-lateral divergence at increased lift ($\alpha > 4°$).

Data obtained during flights B and C, two high Mach number flights, are shown in time-history form in figures 5 and 6, respectively. The tentative plan for each of these flights called for the minimum-drag climb to a moderately high altitude (to reduce the peak dynamic pressure), then a pushover to near level flight for an acceleration run to burnout.

Flight B was a successful high Mach number flight; however, the pushover for the acceleration run was not rapid enough and the airplane reached the peak Mach number of 2.87 while still climbing at a flight-path angle of 4.1°. The performance of flight C was superior to that of flight B because of an additional 12.5 seconds of burning time (which amounted to 5.2 sec at full-rated thrust) and a dive angle of 7° at burnout. Flight C attained a maximum Mach number of 3.20 at an altitude of 65,500 feet.

Burnout of both flights shows effects of asymmetric power conditions consistent with the flight at high altitude.

After power-off for flight B, the airplane remained trimmed at low lift during the deceleration until a Mach number of 2.2 was reached. Directly after burnout of flight C, however, airplane nose-up stabilizer and left-roll aileron were applied to initiate a left turn. As the turn progressed, the stability decreased enough so that the airplane became unstable and uncontrollable. This instability is analyzed in detail in the following section.

The NASA instrumentation ceased to record approximately 15 seconds after the uncontrollable motions were initiated; however, other sources of information (for example, cockpit camera, phototheodolite, crash analysis) indicated that the uncontrolled motions imposed high positive and negative accelerations on the airplane, which finally entered into an inverted spin. The pilot made two recovery attempts, then jettisoned the nose capsule ($t \approx 220$ sec) at a subsonic Mach number and an altitude of approximately 40,000 feet. The separation was clean, with the capsule violently pitching down and imposing a high negative acceleration on the pilot. The deceleration-stabilization parachute deployed and trailed properly, but the pilot could not effect a separation from the capsule and was killed.

Analysis of Airplane Instability

The analysis of the airplane instability experienced during flight C was made by using the internally recorded data, an analog computer, and the aerodynamic derivative coefficients obtained from wind-tunnel and flight data. At the time of flight C, the directional-stability and control-derivative data available for flight guidance were limited to the data shown in figure 7 from references 7, 8, and manufacturer's estimates. A more complete set of wind-tunnel data was obtained following the accident (ref. 9) in order to define the significant derivatives for the higher angle-of-attack and Mach number region of the flight envelope, thereby enabling a more accurate simulation of the motions of the instability.

The directional instability of flight C can be explained as follows: the X-2 remained stable up to a Mach number of 3.20 while at low angles of attack; however, after burnout, control motions were initiated to increase the angle of attack and to produce a left bank (fig. 8 shows an expanded time history). As the speed decreased below $M \approx 3.0$ and the angle of attack simultaneously increased, the directional stability was lowered to such an extent that when corrective aileron was applied to stop the increasing left-bank angle (caused by dihedral effect) the yawing moment resulting from the aileron deflection exceeded the restoring moment caused by sideslip. In addition, the roll due to sideslip was greater than the maximum capability of the ailerons. These motions continued to increase until critical roll velocity for inertial coupling

(calculated to be 1.35 radians per sec for these conditions) was exceeded. At critical roll velocity, violent uncontrollable motions characteristic of inertial coupling occurred about all three axes. It should be noted that although the rudder was locked for flight and there is no evidence that it was unlocked during this flight, the instrumentation indicated a rudder deflection of approximately 1°. This deflection is believed to have been caused by the side forces due to sideslip and is in a direction to aggravate the yawing motions of the airplane. The rudder lock and control-position indicator were both located at the bottom of the rudder, therefore any twisting or bending of the rudder could not be determined.

The value of C_{n_β} required for neutral static directional stability can be expressed for the rudder locked as $C_{n_\beta} = \frac{C_{n_{\delta_a}} C_{l_\beta}}{C_{l_{\delta_a}}}$. The directional-stability coefficient of the X-2 was positive at all times (fig. 9); however, the increase in angle of attack lowered C_{n_β} below the critical value, allowing the control inputs to initiate the divergence. The lower plot of figure 9 shows the ratio of the directional stability to the critical value (based on flight angles of attack and Mach numbers and derivatives of ref. 9) for flights B and C near the peak Mach numbers. Reference 9 presents a similar type of analysis. Although a portion of flight B was in the Mach number range where an instability could occur, the airplane maintained a low angle of attack, with C_{n_β} always greater than the critical value. The ratio of C_{n_β} to the critical value for flight C indicated the airplane to be unstable above a Mach number of 3.1 even though the angle of attack was low. Therefore, an instability before burnout could be expected; however, the divergence did not occur until approximately 20 seconds later when the angle of attack was higher and yawing moments resulting from control action were introduced - thus indicating the flight C_{n_β} was higher than wind-tunnel values, or flight $C_{n_{\delta_a}}$ was lower than wind-tunnel values.

Figure 10 shows a time-history comparison of the directional divergence which occurred during flight C with a programmed six-degree-of-freedom analog simulation of the divergence using modified derivatives obtained from the wind-tunnel data of reference 9. To obtain the comparison it was necessary, as noted previously, to increase the value of C_{n_β} and to decrease the value of $C_{n_{\delta_a}}$ by small amounts.

CONCLUDING REMARKS

During an Air Force program to determine the maximum performance potential of the X-2 research airplane, a maximum Mach number of 3.20 and a maximum geometric altitude of 126,200 feet were attained. Altitudes were attained at which the static and dynamic pressures were 9.4 and 19.1 pounds per square foot, respectively. The aerodynamic controls of the X-2 were effective in changing the airplane attitude during the period of semiballistic flight; however, the flight path was not noticeably changed.

The directionally divergent maneuver which terminated the final high Mach number flight was precipitated by the loss in directional stability that resulted from increasing the angle of attack. The yawing moment from the lateral control was sufficient to initiate the divergence and also to cause, by dihedral effect, rolling moments that were greater than the aileron capabilities of the airplane. The ensuing violent motions resulted from inertial roll coupling.

High-Speed Flight Station,
National Aeronautics and Space Administration,
Edwards, Calif., May 6, 1959.

REFERENCES

1. Weil, Joseph, Comisarow, Paul, and Goodson, Kenneth W.: Longitudinal Stability and Control Characteristics of an Airplane Model Having a 42.8° Sweptback Circular-Arc Wing With Aspect Ratio 4.00, Taper Ratio 0.50, and Sweptback Tail Surfaces. NACA RM L7G28, 1947.

2. Turner, Thomas R., Lockwood, Vernard E., and Vogler, Raymond D.: Aerodynamic Characteristics at Subsonic and Transonic Speeds of a 42.7° Sweptback Wing Model Having an Aileron With Finite Trailing-Edge Thickness. NACA RM L8K02, 1949.

3. Spearman, M. Leroy, and Robinson, Ross B.: The Aerodynamic Characteristics of a Supersonic Aircraft Configuration With a 40° Sweptback Wing Through a Mach Number Range From 0 to 2.4 as Obtained From Various Sources. NACA RM L52A21, 1952.

4. Day, Richard E.: Measurements Obtained During the Glide-Flight Program of the Bell X-2 Research Airplane. NACA RM L53G03a, 1953.

5. Zalovcik, John A.: A Radar Method of Calibrating Airspeed Installations of Airplanes in Maneuvers at High Altitudes and at Transonic and Supersonic Speeds. NACA TN 1979, 1949.

6. Warfield, Calvin N.: Tentative Tables for the Properties of the Upper Atmosphere. NACA TN 1200, 1947.

7. Spearman, M. Leroy, and Palazzo, Edward B.: An Investigation of a Supersonic Aircraft Configuration Having a Tapered Wing With Circular-Arc Sections and 40° Sweepback - Static Longitudinal and Lateral Stability and Control Characteristics at a Mach Number of 1.89. NACA RM L54G26a, 1954.

8. Ellis, Macon C., Jr., Hasel, Lowell E., and Grigsby, Carl E.: Supersonic-Tunnel Tests of Two Supersonic Airplane Model Configurations. NACA RM L7J15, 1947.

9. Fournier, Roger H., and Silvers, H. Norman: Investigation of the Static Lateral Stability and Aileron Characteristics of a 0.067-Scale Model of the Bell X-2 Airplane at Mach Numbers of 2.29, 2.78, 3.22, and 3.71. NACA RM L57J28a, 1958.

TABLE I.- PHYSICAL CHARACTERISTICS OF THE X-2 AIRPLANE

Wing:	
Area, sq ft	260.4
Span, ft	32.3
Aspect ratio	4
Taper ratio	0.5
Sweep at quarter chord, deg	40
Mean aerodynamic chord, ft	8.379
Location of mean aerodynamic chord, horizontal from fuselage center line, in.	79.42
Airfoil section	10-percent-thick circular arc
Incidence -	
Root, deg	3
Tip, deg	3
Dihedral, deg	3
Root chord, ft	10.765
Aileron:	
Area, sq ft	10.8
Travel, deg	±17
Trailing-edge thickness	50 percent of thickness at 80-percent wing chord
Flap, trailing edge:	
Area (total), sq ft	21.2
Travel, deg	45
Flap, leading edge:	
Area (total), sq ft	12.2
Travel, leading edge down, deg	15
Horizontal tail:	
Area, sq ft	43.7
Span, ft	12.83
Aspect ratio	3.75
Sweep at quarter chord, deg	40.0
Airfoil section	NACA 65008
Mean aerodynamic chord, ft	3.571
Travel, deg -	
Leading edge up	7
Leading edge down	10
Vertical tail:	
Area, sq ft	38.6
Span, ft	6.71
Aspect ratio	1.17
Sweep at quarter chord, deg	32.5
Airfoil section -	
Root	NACA 27010
Tip	NACA 27008
Mean aerodynamic chord, ft	7.067
Rudder -	
Area, sq ft	6.9
Travel, deg	±30
Fuselage:	
Length, ft	37.83
Frontal area, sq ft	13.75
Fineness ratio	9.5
Landing gear:	
Area of main skid, sq in.	400
Airplane weight, lb:	
Launch (full rocket fuel)	24,910
Landing (without rocket fuel)	12,375
Moments of inertia:	
I_X, slug-ft^2	$0.137m + 4,990$
I_Y, slug-ft^2	$36.6m + 11,420$
I_Z, slug-ft^2	$39.0m + 14,130$
I_{XZ}, slug-ft^2	$800 - 0.000825(m - 530)^2$

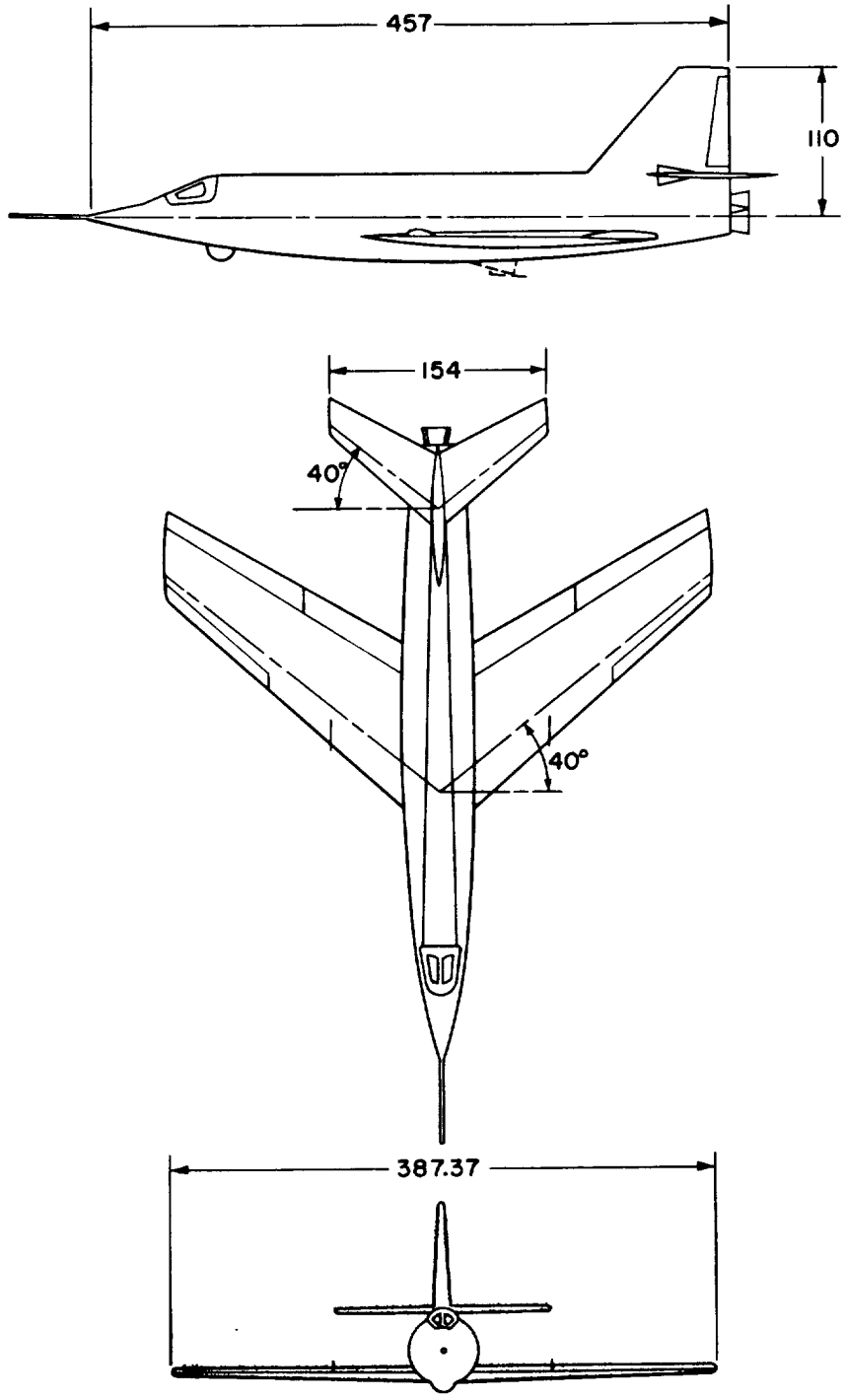

Figure 1.- Three-view drawing of X-2 research airplane. All dimensions in inches.

Figure 2.- Side view of the X-2 research airplane. L-59-3001

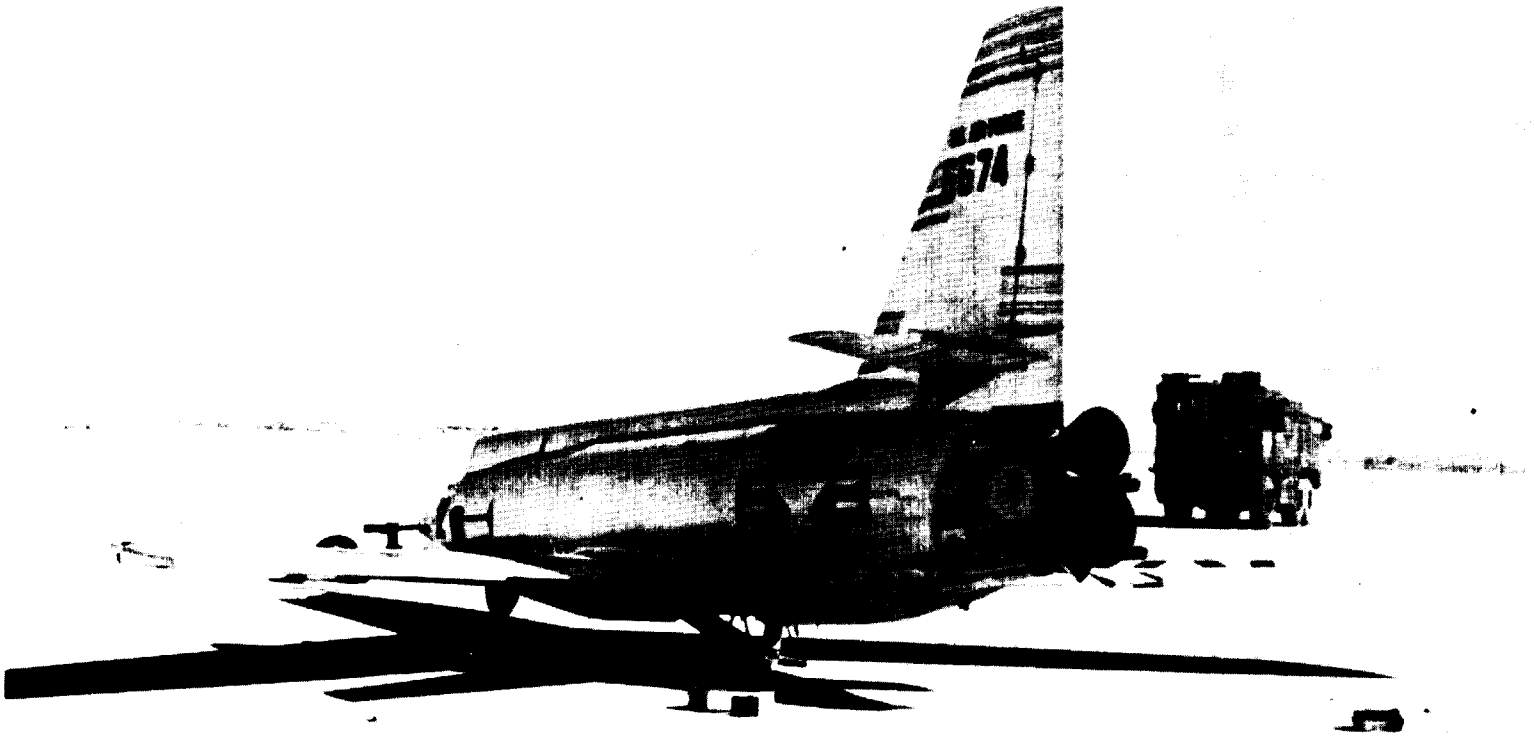

Figure 3.- Three-quarter rear view of the X-2 research airplane. L-59-3002

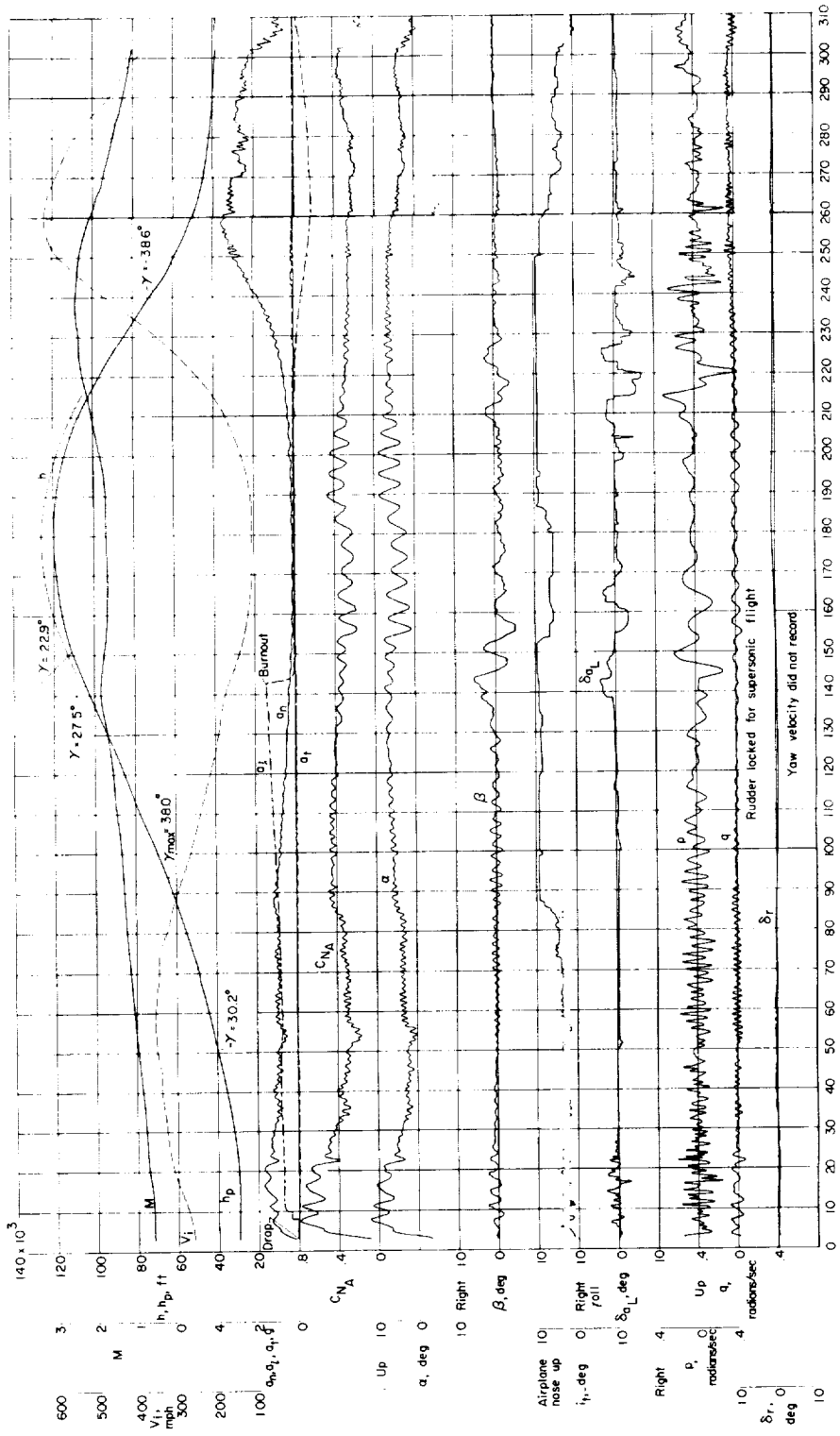

Figure 4.- Time history of flight A, the maximum-altitude flight of the X-2 airplane.

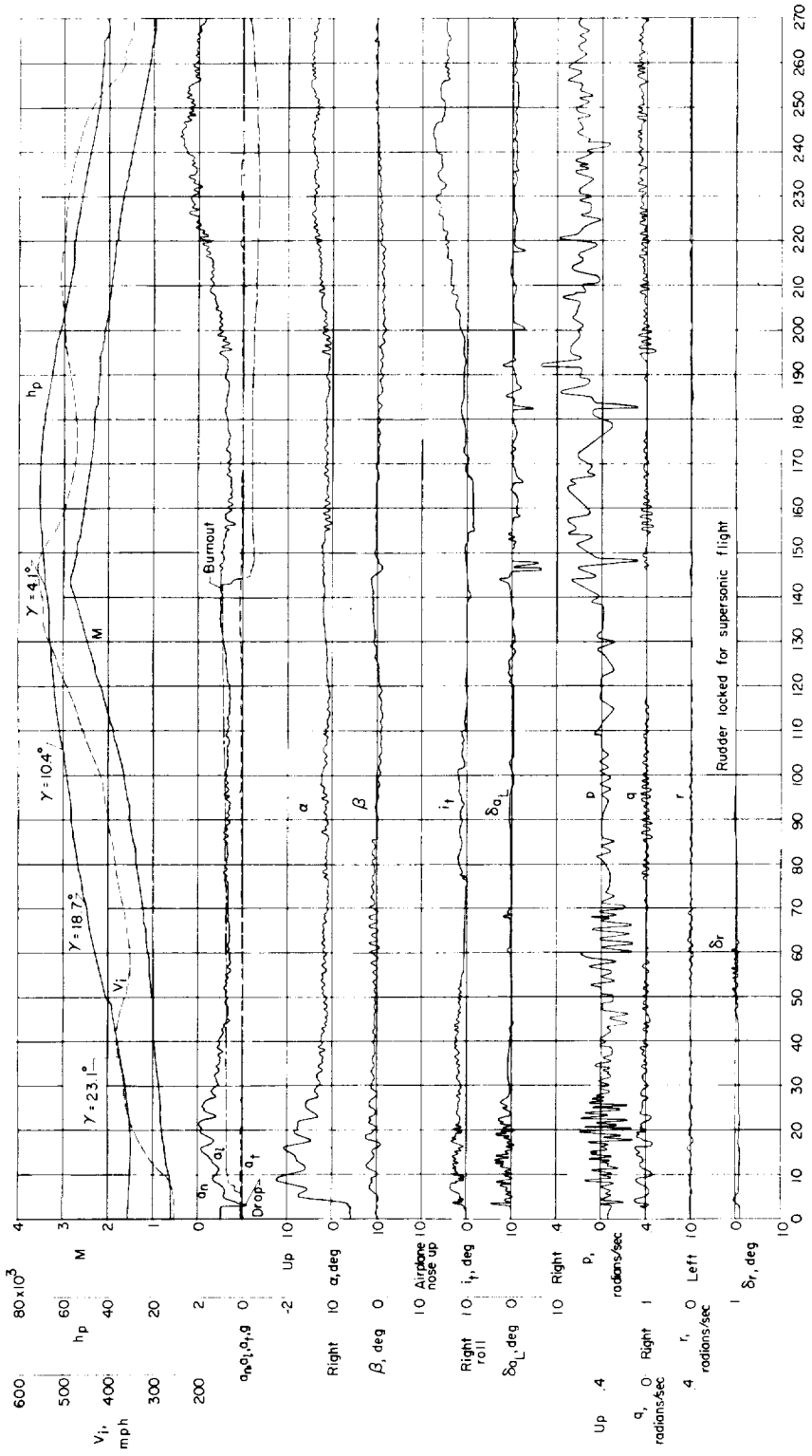

Figure 5.- Time history of flight B, high Mach number flight of the X-2 airplane.

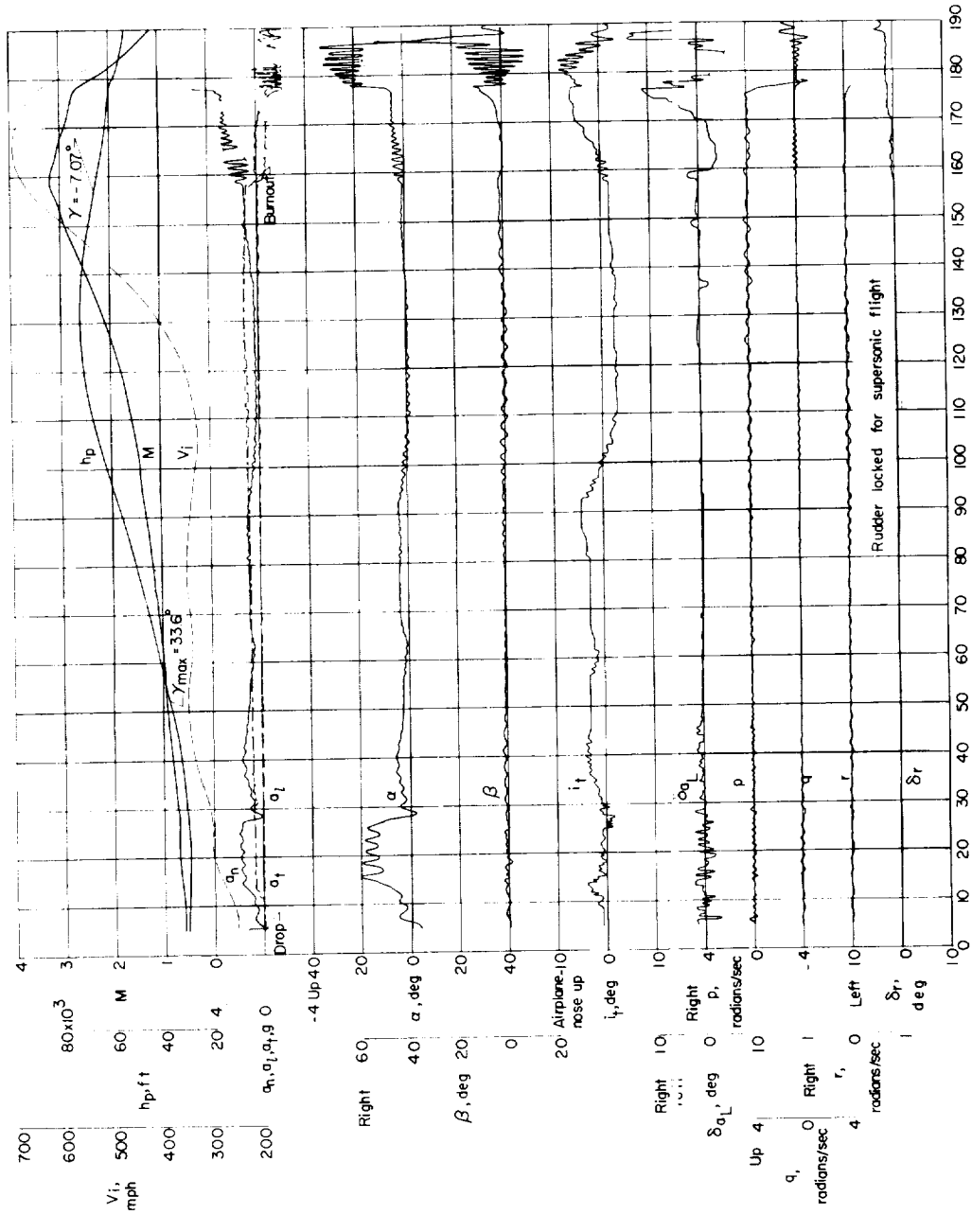

Figure 6.- Time history of flight C, high Mach number flight of the X-2 airplane. Gaps in record result from film exposure to sunlight.

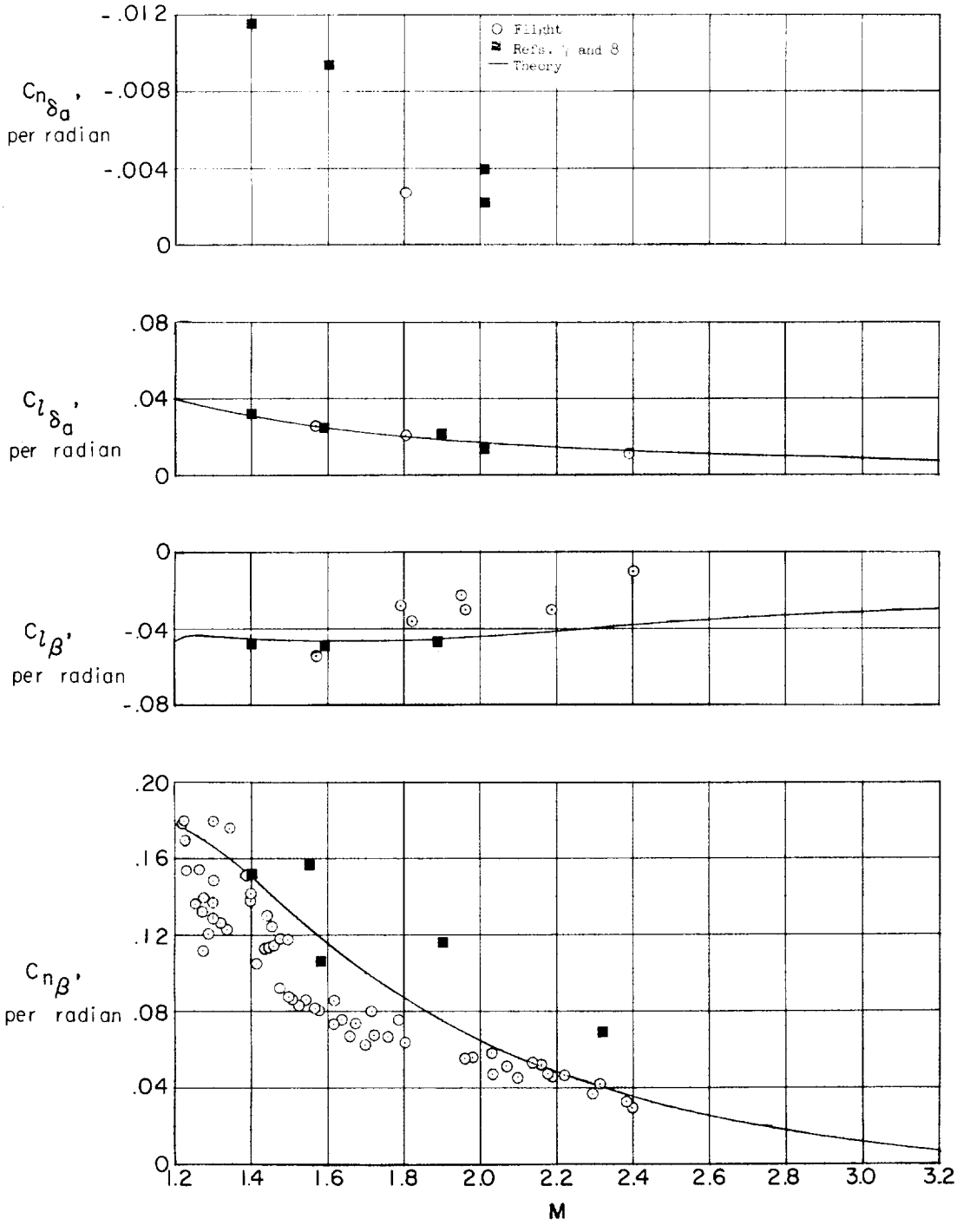

Figure 7.- Stability and control derivative data available at time of flight C.

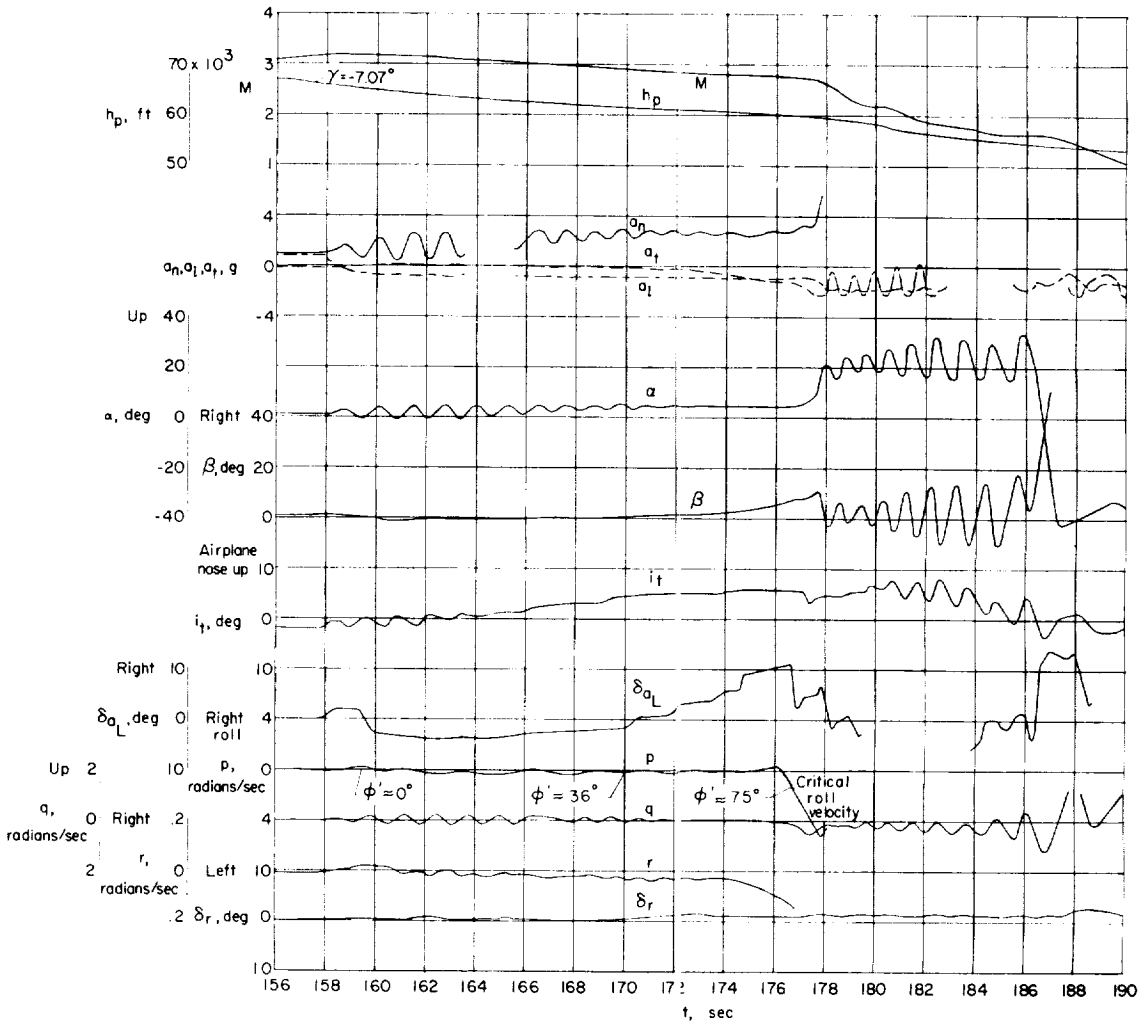

Figure 8.- Expanded plot of flight C showing directional divergence. Gaps in record result from film exposure to sunlight.

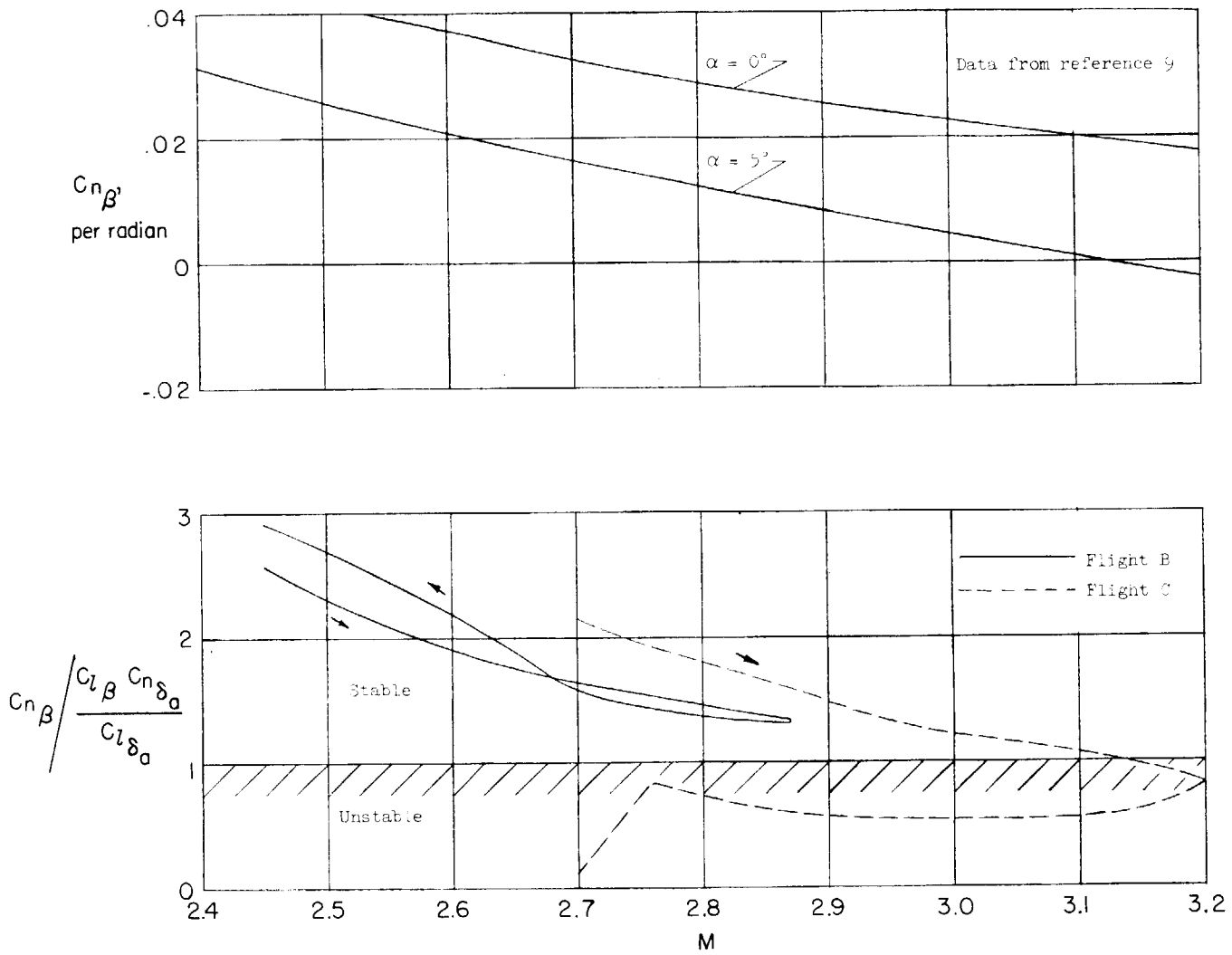

Figure 9.- Directional-stability data of high Mach number flights using wind-tunnel derivatives for flight conditions.

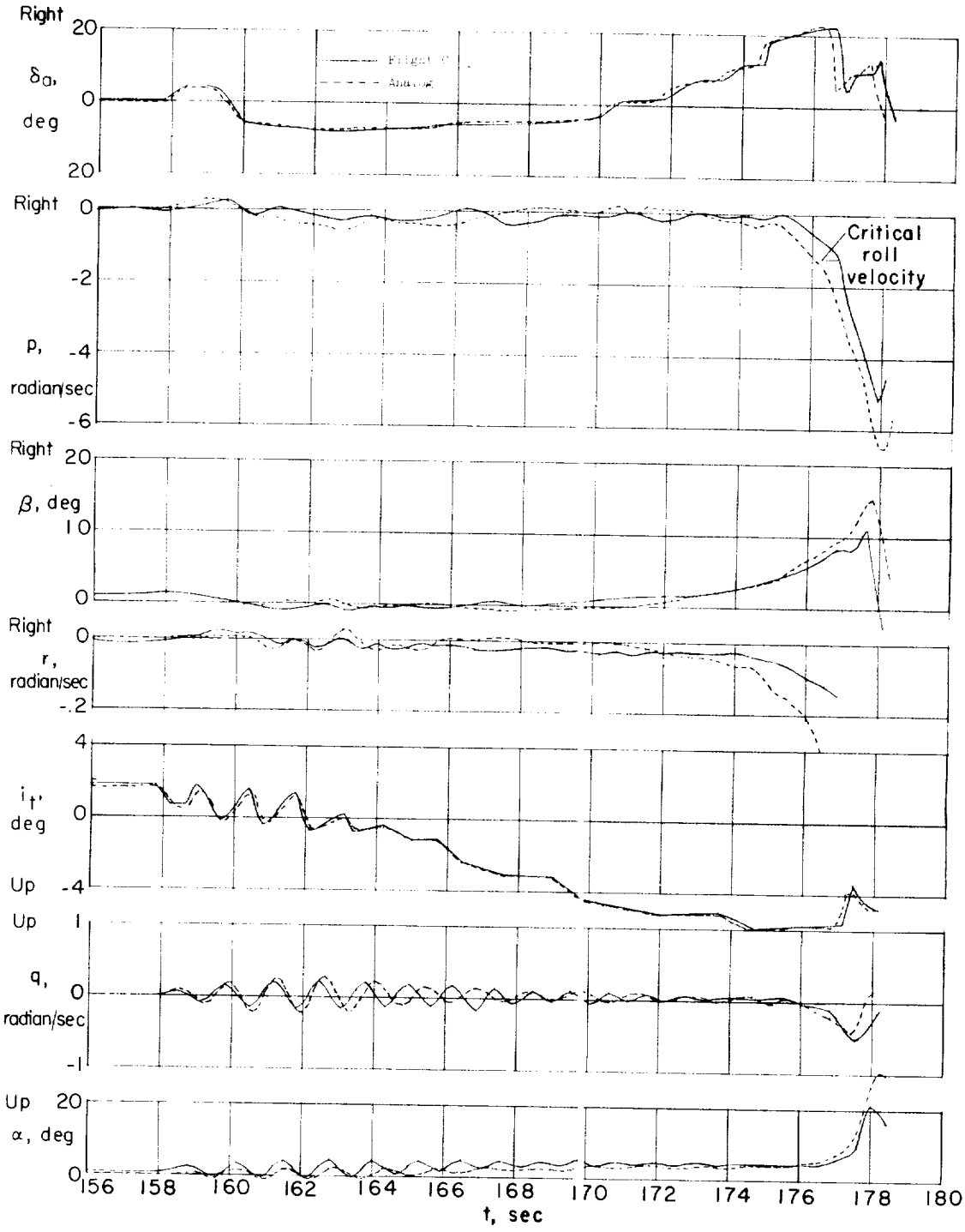

Figure 10.- Comparison of directional divergence of flight C with analog simulation.